

1	<b>TITLE</b>
2	<b>INVESTIGATOR(S)</b>
3	<b>INTRODUCTION</b>
4	<b>THEORY OF ALGORITHM/MEASUREMENTS</b>
5	<b>EQUIPMENT</b>
6	<b>PROCEDURE</b>
7	<b>OBSERVATIONS</b>
8	<b>DATA DESCRIPTION</b>
9	<b>DATA MANIPULATIONS</b>
10	<b>ERRORS</b>
11	<b>NOTES</b>
12	<b>REFERENCES</b>
13	<b>DATA ACCESS</b>
14	<b>OUTPUT PRODUCTS AND AVAILABILITY</b>
15	<b>GLOSSARY OF ACRONYMS</b>
16	<b>UMD UPDATES</b>

## **1. TITLE**

### **1.1 Data Set Identification**

Global Inventory Modeling and Mapping Studies (GIMMS) Satellite Drift Corrected and NOAA-16 incorporated Normalized Difference Vegetation Index (NDVI), Monthly 1981–2006.

### **1.2 Database and Database Table Name(s)**

Not applicable to this data set.

### **1.3 File Name(s)**

The files in this data set are named using the following naming convention:

**AF03dec15a.n16-VIg**

where

**AF** identifies the continent

AF = Africa

AZ = Australia and New Zealand

EA = Eurasia

NA = North America

SA = South America and Central America

The global mosaic files created by GLCF do not have this prefix

**03** is the two digit year,

**1981** to 2006.

**dec** is abbreviated month from January to December.

**15a** identifies the composite period, 15a denotes the days 1-15 of the month, and 15b denotes the days from 16 to the end of the month (28, 30 or 31).

**n16** identifies the satellite, NOAA-7, 9, 11, 14, 16, or 17 from which the data originated.

**VIg** identifies the data type, here NDVI.

### **1.4 Data Access**

This data collection is available for free via FTP at the Global Land Cover Facility (GLCF) [www.landcover.org](http://www.landcover.org). To access the data go to <http://glcf.umiacs.umd.edu/data/gimms/>.

*Global Inventory Modeling and Mapping Studies (GIMMS) AVHRR 8km Normalized Difference Vegetation Index (NDVI), Bimonthly 1981-2006.*

## 1.5 Revision Date of this Document

October 15, 2007.

## 2. INVESTIGATOR(S)

### 2.1 Investigator's Name and Title

Jorge E. Pinzon and Molly E. Brown  
Science Systems and Applications  
NASA-Goddard Space Flight Center  
Code 614.4  
Greenbelt, MD 20771

Compton J. Tucker  
NASA-Goddard Space Flight Center  
Code 610  
Greenbelt, MD 20771

### 2.2 Title of Investigation

Monitoring Seasonal and interannual variations in Land-Surface Vegetation from 1981-2006 using GIMMS NDVI.

### 2.3 Contacts (For Data Production Information)

	Contact 1	Contact 2
<b>2.3.1 Name</b>	Dr. Molly E. Brown	Dr. Jorge E. Pinzon
<b>2.3.2 Address City/St. Zip Code Country</b>	NASA-Goddard Space Flight Center Code 923  Greenbelt, MD 20771 USA	NASA-Goddard Space Flight Center Code 923  Greenbelt, MD 20771 USA
<b>Tel. No. Fax No.</b>	301-614-6616 301-614-6015	301-614-6685 301-614-6015
<b>E-mail</b>	<a href="mailto:molly.brown@nasa.gov">molly.brown@nasa.gov</a>	<a href="mailto:jorge_pinzon@ssaihq.com">jorge_pinzon@ssaihq.com</a>

### 2.4 Requested Form of Acknowledgment

Please cite the following publications whenever these data are used:

Pinzon, J., Brown, M.E. and Tucker, C.J., 2005. Satellite time series correction of orbital drift artifacts using empirical mode decomposition. In: N. Huang (Editor), Hilbert-Huang Transform: Introduction and Applications, pp. 167-186.

Tucker, C.J., Pinzon, J.E., Brown, M.E., Slayback, D., Pak, E.W., Mahoney, R., Vermote, E. and Saleous, N., 2005. An Extended AVHRR 8-km NDVI Data Set Compatible with MODIS and SPOT Vegetation NDVI Data. International Journal of Remote Sensing, 26(20): 4485-4498.

*Global Inventory Modeling and Mapping Studies (GIMMS) AVHRR 8km Normalized Difference Vegetation Index (NDVI), Bimonthly 1981-2006.*

### 3.0 Introduction

#### 3.1 Objective/Purpose

The Global Inventory Modeling and Mapping Studies (GIMMS) normalized difference vegetation index (NDVI) data sets were generated to provide a 25-year satellite record of monthly changes in terrestrial vegetation. New features of this dataset include reduced NDVI variations arising from calibration, view geometry, volcanic aerosols, and other effects not related to actual vegetation change. In particular, NOAA-9 descending node data from September 1994 to January 1995, volcanic stratospheric aerosol correction for 1982-1984 and 1991-1994, and improved NDVI using empirical mode decomposition/reconstruction (EMD) to minimize effects of orbital drift. Global NDVI was generated to provide inputs for computing the time series of biophysical parameters contained in the International Satellite Land Surface Climatology Project (ISLSCP) Initiative II collection. NDVI is used in climate models and biogeochemical models to calculate photosynthesis, the exchange of CO<sub>2</sub> between the atmosphere and the land surface, land-surface evapotranspiration and the absorption and release of energy by the land surface.

#### 3.2 Summary of Parameters

Global, composited, monthly, normalized difference vegetation index over land areas. NDVI is the difference (in reflectance) between the AVHRR near-infrared and visible bands divided by the sum of these two bands (Tucker 1980; Sellers 1985; Sellers et al. 1994).

#### 3.3 Discussion

Because NDVI is a ratio of differences between two adjacent bands, it is largely *insensitive* to variations in illumination intensity. However, NDVI *is sensitive* to effects that differ between bands. Band calibrations, for example, have changed frequently between the five NOAA AVHRR instruments that acquired the NDVI record for the 22-year Initiative II period. In addition, natural variability in atmospheric aerosols and column water vapor have affected the NDVI record. Over the period of record there were two major volcanic eruptions, El Chichon in 1982 and Mt. Pinatubo in 1991, which injected large quantities of aerosols into the Earth's stratosphere. These aerosols, along with smoke from biomass burning and dust from soil erosion and other factors, can introduce significant variability in the AVHRR NDVI record. These constituents have significantly different effects on AVHRR band's 1 and 2. The GIMMS NDVI corrects for the known changes of the atmosphere from these two volcanic eruptions, but reductions in the NDVI signal can still be seen over densely vegetated tropical land covers for limited time periods.

NDVI is also sensitive to the periodic variations in solar illumination angle and sensor view angles induced by the NOAA orbits. Its polar, sun-synchronous orbits permitted daily coverage of each point on earth, although at time-varying viewing and illumination geometry. The GIMMS NDVI dataset has a satellite overpass time drift correction that largely eliminates the variation of NDVI due to changes in solar zenith angle.

Frequent cloud cover can also create numerous gaps in the daily AVHRR record eliminating roughly two thirds of the data. In order to construct cloud-free views of the Earth, composite images were constructed at regular intervals by selecting pixels with the maximum NDVI during regularly spaced intervals. Choosing pixels with maximum NDVI reduces cloud cover and water vapor effects since both strongly reduce NDVI. Compositing can be done over any time interval, but 9-10 days is generally selected as the minimum period since the NOAA

orbit repeats at that frequency. The GIMMS data record constructed here is based on 15-day composites. There are two 15-day composites per month, the first for day 1-15, and the second for day 16 to the end of the month.

#### **4. THEORY OF ALGORITHM/MEASUREMENTS**

Green leaves have a higher reflectance in the AVHRR near infrared band (band 2) than in the visible band (band 1), because of differences in leaf chlorophyll absorption between the two bands. Chlorophyll absorbs strongly in the red region, spanned by AVHRR band 1. Thus, the difference in vegetation reflectance between the near infrared and visible bands increases with green leaf vegetation density, hence chlorophyll concentration. The ratio of the difference between band 2 and band 1 and their sum, hence the NDVI, is an index that ranges between -1 and +1; the observed range is usually smaller: Non-vegetated materials generally have a much lower NDVI (around 0) than dense vegetation (>0.7), since their near infrared and visible reflectances are more nearly equal.

#### **5. EQUIPMENT**

##### **5.1 Instrument Description**

The Advanced Very High Resolution Radiometer (AVHRR) acquired data in 5 spectral bands; one visible, one near infrared and three thermal bands, all with 1024 quantizing levels. The thermal bands are not used in the GIMMS NDVI data. The AVHRR produces at 1.1 and 4 km spatial resolution. The 4-km product or global area coverage (GAC) product is derived from the 1-km product by onboard sampling. The 4-km product is available globally from July 1981 until the present. The 1-km record is not continuous. Its availability depends upon prior arrangements made by NOAA, or on the proximity of a local receiving station that can capture the data directly from the satellite. See NOAA –KLM users guide for specifications of the newest NOAA AVHRR instruments. <http://www2.ncdc.noaa.gov/docs/klm/>

##### **5.1.1 Platform**

The NOAA AVHRR satellite series 7, 9, 11, 14, and 16 used for this NDVI record flew in sun-synchronous polar orbits with a nominal 1:30 or 2:30 PM local daytime overpass time at launch. However, the overpass times drifted by 1-2 minutes per month to as much as 4 1/2 hours later in the day creating variable illumination and view angles over the period of record. The 55-degree sensor swath width permitted a daily view of each pixel on Earth although at different illumination and view angles during the 9-day repeat cycle. Maximum value NDVI data compositing tends to select pixels acquired in a near-nadir mode with minimum atmospheric effects. Even so, view, illumination and atmospheric effects remain. Reducing these effects was the aim of GIMMS processing.

##### **5.1.2 Mission Objectives**

The NOAA AVHRR satellite sensor series was originally designed as a weather satellite. However from the early 1980s, AVHRR data has found increasing use to monitor the type and condition of land vegetation. AVHRR vegetation data archives extend back to August 1981.

##### **5.1.3 Key Variables**

The AVHRR measured top of the atmosphere radiance in 5 bands. Band 1 covered the 0.5 to 0.7 um region, band 2 the 0.7 to 1.1 um region, with three thermal bands one covering the middle infrared region around 3 microns and two thermal infrared bands in the 10 to 11 micron region. The GIMMS NDVI product uses as input radiance in bands 1 and 2 and were mapped at the NASA

Goddard Space Flight Center under the guidance of Dr. Compton Tucker. The current adjusted NDVI dataset was derived entirely from the NDVI produced during the 1998-2000 remapping effort of the GIMMS group.

#### **5.1.4 Principles of Operation**

The NOAA satellite series, NOAA 6, 7, 9, 11, 14, 16 and 17 were in polar, sun-synchronous orbits with nadir afternoon overpass times. NOAA 7 data span the years 1981 -1985, NOAA 9, 1986-1989, NOAA 11, 1989-1995, NOAA 14, 1995-2000, and NOAA-16 from 2000 to 2003, and NOAA-17 from 2004 to 2006. Data from NOAA-9 was used from September 1994 until January 1995 when NOAA 11 started to malfunction and its replacement, NOAA 13, failed shortly after launch. Each AVHRR sensor has different and variable calibration and overpass time.

#### **5.1.5 Instrument Measurement Geometry**

The AVHRR is a scanning, imaging radiometer, scanning  $\pm 55$  degrees, providing a 2800 km swath width. The orbital configuration permits daily coverage at a maximum spatial resolution of 1 km of each point on earth, although at different viewing and illumination geometries on subsequent days. The orbit repeats its ground track each 9 days.

#### **5.1.6 Manufacturer of Instrument**

See NOAA –KLM users guide for specifications of the newest NOAA AVHRR instrument. <http://www2.ncdc.noaa.gov/docs/klm/>

### **5.2 Calibration**

NOAA provides preflight calibration coefficients that relate the digital counts measured by the satellite to reflectances. The preflight calibration coefficients for the visible and near infrared channel are of the following form:

$$\text{reflectance} = \text{gain} * (\text{digital counts} - \text{offset})$$

The gain and the offset are determined on the ground prior to launch of the satellite; The gain and offset are referred to as preflight calibration coefficients. The preflight calibration coefficients change for each satellite. In some cases preflight coefficients were updated during the time of operation of a satellite.

Preflight calibration coefficients do not take into account the degradation of the AVHRR during its time of operation. Several techniques exist to correct for the change in sensitivity of the AVHRR. For the GIMMS data, the coefficients by Vermote and Kaufman (1995) are used to correct the visible and near infrared reflectances for in-flight sensor degradation. In the GIMMS NDVI data the relative degradation error in the gain is further reduced to below 1 % by using a desert calibration of the ratio of channels 1 and 2 reflectances to invariant Sahara Desert targets.

#### **5.2.1 Specifications**

##### **5.2.1.1 Tolerance**

See Vermote and Kaufman (1995) and Section 9.2.1 for more details.

#### **5.2.2 Frequency of Calibration**

See Vermote and Kaufman (1995) and Section 9.2.1 for more details. (Vermote and Kaufman 1995)

### 5.2.3 Other Calibration Information

See Rao and Chen (1995). (Rao and Chen 1995)

## 6. PROCEDURE

### 6.1 Data Acquisition Methods

The input data for the GIMMS Land data processing is the NOAA AVHRR GAC 1B data. Our GAC 1B data were obtained from NOAA and from NCAR sources at the time of acquisition from 1985 to the present. We have augmented this dataset with GAC 1B data available from NOAA's Satellite Active Archive now called CLASS. The GIMMS NDVI datasets were corrected using solar zenith angle values from the AVHRR sensor for the period of 1981-2002 (Pinzon 2002; Pinzon et al. 2004; Tucker et al. 2005).

### 6.2 Spatial Characteristics

#### 6.2.1 Spatial Coverage

The coverage is global for all land areas except Greenland and Antarctica.

#### 6.2.2 Spatial Resolution

The data are given in an 8km Albers Equal Area Conic projection, Clarke 1866 ellipsoid, and in geographic coordinates, WGS84 datum at 0.07272727 degree resolution per pixel. .

### 6.3 Temporal Characteristics

#### 6.3.1 Temporal Coverage

The data are available from July 1981 through December 2006.

#### 6.3.2 Temporal Resolution

Monthly; the GIMMS dataset is composited at a 15-day time step. The 15a composite is the maximum value composite from the first 15 days of the month, and the second (15b) is from days 16 through the end of the month.

## 7. OBSERVATIONS

### 7.1 Field Notes

Not applicable to this dataset.

## 8. DATA DESCRIPTION

### 8.1 Table Definition with Comments

Not applicable to this dataset.

### 8.2 Type of Data

8.2.1 Parameter/ Variable Name	8.2.2 Parameter/ Variable Description	8.2.3 Data Range	8.2.4 Units of Measurement	8.2.5 Data Source
--------------------------------------	---	---------------------	-------------------------------	-------------------------

*University of Maryland Global Land Cover Facility Data Distribution*

GIMMS NDVI	GIMMS* Normalized Difference Vegetation Index calculated+ From AVHRR channel 1 and 2 digital count data.	Theoretical range between -1 and 1; values around 0 for bare soil (low or no vegetation) values of 0.7 or larger for dense vegetation. Water= -0.1 No Data = -0.05	[Unitless]	AVHRR
------------	--	--	------------	-------

\*GIMMS Normalized Difference Vegetation Index has been corrected for:

- residual sensor degradation and sensor intercalibration differences;
- distortions caused by persistent cloud cover globally;
- solar zenith angle and viewing angle effects due to satellite drift;
- volcanic aerosols;
- missing data in the Northern Hemisphere during winter using interpolation due to high solar zenith angles;
- low signal to noise ratios due to sub-pixel cloud contamination and water vapor.

### 8.3 Sample Data Record

Not applicable to this dataset.

### 8.4 Data Format

The original data are 8km resolution continental files, Albers projection, with flags embedded. The GLCF converted the files from native binary to GeoTIFF format. To extract the flags use the following formula:

$$FLAG = \text{raw} - \text{floor}(\text{float}(\text{raw})/10) * 10$$

NDVI values have been scaled to values ranging from -1000 to 1000, water pixels are assigned the value of -10000, and masked pixels are -5000. To recover the NDVI range of -1 to 1 use the following formula:

$$NDVI = \text{float}(\text{raw}/10000)$$

The continental files have the following numbers of columns and rows:

SA = South America	1152 x 1152
AF = Africa	1152 x 1152
NA = North America	1024 x 1280
EA = Eurasia	2000 x 1250
AZ = Australia/New Zealand	1152 x 864

The center of the corner pixels for the Albers continental files are the following ( in degrees):

	Africa	South America	North America	Eurasia	Australia New Zealand
Lower left lat	-42.243	-54.609	-2.417	-28.732	-45.708
Lower left lon	-23.49	-120.024	-143.913	19.336	73.003
Upper left lat	43.711	31.448	54.626	34.609	14.836

*Global Inventory Modeling and Mapping Studies (GIMMS) AVHRR 8km Normalized Difference Vegetation Index (NDVI), Bimonthly 1981-2006.*

### *University of Maryland Global Land Cover Facility Data Distribution*

Upper left lon	-24.6	-99.665	157.412	-50.358	92.873
Lower right lat	-42.242	-54.635	-2.382	-28.67	-45.736
Lower right lon	63.414	-7.069	-62.143	130.62	-173.093
Upper right lat	43.712	31.43	54.686	34.675	14.816
Upper right lon	64.523	-27.396	-3.476	-159.665	167.065

The GLCF files are global mosaics, in lat-lon projection and 0.07272727 degrees spatial resolution, with separate flag files, identical to the flag values in the continental data. No formula is needed for these. The global mosaic files are also in GeoTIFF format.

The global mosaic files have the following number of columns and rows:

Global mosaics                      4950 x 2091

The center of the corner pixels for the global mosaic files are the following (in degrees):

	Global
Lower left lat	-62.813
Lower left lon	-179.959
Upper left lat	89.187
Upper left lon	-179.959
Lower right lat	-62.813
Lower right lon	179.968
Upper right lat	89.187
Upper right lon	179.968

### **Flag files**

The flag values have the following meaning for both data sets:

FLAG = 6 (missing data)

FLAG = 5 (NDVI retrieved from average seasonal profile, possibly snow)

FLAG = 4 (NDVI retrieved from average seasonal profile)

FLAG = 3 (NDVI retrieved from spline interpolation, possibly snow)

FLAG = 2 (NDVI retrieved from spline interpolation)

FLAG = 1 (Good value, possibly snow)

FLAG = 0 (Good value)

### **8.5 UMD Updates**

The Global Land Cover Facility, University of Maryland Institute for Advanced Computer Studies.

[www.landcover.org](http://www.landcover.org)

Paul Davis, Matthew Smith, Kuan Song

October 15, 2007

#### **8.5.1 Objectives**

In order to facilitate access to the data the GLCF stitched all continental files to create a single global mosaic file for each date. The data was reprojected to Geographic coordinates to facilitate access for GIS users. A rigorous reprojection procedure was used instead of

*Global Inventory Modeling and Mapping Studies (GIMMS) AVHRR 8km  
Normalized Difference Vegetation Index (NDVI), Bimonthly 1981-2006.*

*University of Maryland Global Land Cover Facility Data Distribution*  
warping, yielding higher accuracy. The resampling scheme is nearest neighbor and the pixel resolution is 0.07272727.

### **8.5.2 Mosaic**

A “North over South” scheme was used to create the global mosaics, meaning that if one location had a valid value in both the North America tile and South America tile, the North America tile was used because of less cloud probability.

### **8.5.3 Data-Flag Separation**

The GLCF extracted the flag data from the original files and offers the NDVI and flag data as separate files.

### **8.5.4 Previews and Metadata**

The GLCF also produced browse and preview JPEG images that can be download along with the data. Additionally, a text file that includes basic metadata is also available.

### **8.5.5 Formats**

The global mosaic versions of the NDVI and flag data are available as two separate 16-bit GeoTIFF files in geographic coordinates. The data are also available in the original Albers Equal Area projection, but the files were converted from binary to GeoTIFF format. Each continental file contains both the NDVI and flag data embedded in one file, and the appropriate values can be extracted using the formulas listed above.

## **8.6 Related Data Sets**

The 8 km GIMMS Land Surface AVHRR data set (Tucker et al. 2005) is available at its original spatial resolution directly from the GIMMS group. Please contact Dr. Tucker for this dataset. LAI and FPAR fields at quarter degree resolution based on the GIMMS data are also available.

## **9. DATA MANIPULATIONS**

### **9.1 Formulas**

#### **9.1.1 Derivation Techniques/Algorithms**

See Section 9.2.1.

### **9.2 Data Processing Sequence**

#### **9.2.1 Processing Steps and Data Sets**

The 8 km fields from the GIMMS Land Surface AVHRR data set available are (Tucker et al. 2005) :

- NDVI
- solar zenith angle
- Temperature Channel 4
- Temperature Channel 5

#### **9.2.3 8-km NDVI Data Processing**

Satellite data in NOAA level-1b format (Kidwell 1998) were ingested from magnetic media, were forward mapped to the output bin closest to the center location of each 8 km equal area grid

*Global Inventory Modeling and Mapping Studies (GIMMS) AVHRR 8km  
Normalized Difference Vegetation Index (NDVI), Bimonthly 1981-2006.*

cell, respective calibration values were applied to each channel (Vermote and Kaufman 1995), and the other values associated with the maximum NDVI were retained for each compositing period. Data from seven AVHRR instruments on different satellite platforms were used in this dataset (Table 1).

**Table 1. Instrument change times for the GIMMS dataset.**

AVHRR instrument	Start date	End date
NOAA-7	July 1, 1981	February 8, 1985
NOAA-9	February 11, 1985	November 7, 1988
NOAA-11	November 11, 1988	September 19, 1994
NOAA-9 (descending)	September 20, 1994	January 18, 1995
NOAA-14	January 19, 1995	October 31, 2000
NOAA-16	November 1, 2000	December 31, 2003
NOAA-17	January 1, 2004	continuing

We used a similar navigation procedure to El Saleous *et al.* (2000), which in turn is based upon the work of Baldwin and Emery (1995). The orbital model predicts the position of the satellite at any time, using the satellite on-board clock and orbital elements to determine the predicted position. From this perspective, the sun-target-sensor geometry is determined. The NOAA satellites' velocity with respect to the earth's surface is ~7 km/second and the output bin size we employed is 8 km. This translates into a timing error of ~1.0 second to achieve a navigation accuracy of  $\leq 1$  pixel. The majority of our navigation errors were due to errors of the on-board spacecraft clock. (El Saleous *et al.* 2000) (Baldwin and Emory 1995)

Every composite image was manually checked for navigation accuracy by comparing the mapped data to a reference coastline for the continent in question. Images with  $> 1$  pixel navigation error were investigated and the day(s) of the navigation error identified. These days were subsequently reprocessed separately and manually registered to the reference data, to bring the badly navigated day(s) into agreement with the reference coastline, and the composite image was reconstructed by maximum value NDVI compositing. In a few cases it was necessary to discard data from specific days, as the navigation errors were impossible to adjust.

With the failure of NOAA-13 to achieve orbit in 1992, NOAA-11 continued to provide global afternoon/early morning AVHRR data. By 1994, the afternoon equatorial overpass time for NOAA-11 was ~ 17:00 hours. We began using NOAA-9 descending node AVHRR data for our global NDVI data set in September 1994, and continued using these data until NOAA-14 became operational in late January 1995<sup>1</sup>. There is thus a fundamental difference between the PAL and GVI data sets and the data set we describe herein: We use NOAA-9 AVHRR data from October 1994 into January 1995 when there were no NOAA-11 AVHRR data (it had failed), and use NOAA-9 AVHRR data in September 1994 when the PAL and GVI data sets use NOAA-11 data.

### **9.2.3.1 Radiometric calibration**

Satellite determination of long-term surface trends requires precision within and among various space-borne instruments. It is also crucial to document the within- and among-sensor

<sup>1</sup> NOAA-9 had a day-time descending node equatorial crossing time of ~09:00 hours in mid-1994 to early 1995. It had "rocked around the clock", with a ~2-3 minute/month later time procession from its original day time descending node equatorial crossing time of 02:30 hours.

calibration uncertainty to determine the accuracy with which surface trends over time can be ascertained. The NDVI data we describe were processed in two ways: (1) NOAA-7 through NOAA-14 channel 1 and 2 data from were processed using the Vermote and Kaufman (1995) channel 1 and channel 2 calibration. The resulting NDVI fields were further adjusted using the technique the desert calibration technique from Los (1998), then decomposed and reconstructed using empirical mode decomposition to correct for solar zenith angle effects (Pinzon 2002) and (2) Data from NOAA-16 were processed using the preflight channel 1 and channel 2 calibration values and formed into maximum values composites. An empirical mode decomposition and reconstruction was performed to insure a slope with respect to time of 0.00 in desert areas and was also used to correct solar zenith angle artifacts. This NOAA-16 NDVI time series was adjusted by a constant offset to match up with a coincident-in-time and spatially-aggregated 8-km SPOT Vegetation NDVI time series, which had previously been adjusted to match up with the corresponding coincident-in-time NOAA-14 NDVI time series. We thus used overlapping SPOT Vegetation NDVI time series as the means to intercalibrate or tie together the NOAA-14 and NOAA-16 NDVI time series (Pinzon et al. 2004). This was necessary because the bi-linear gain for channel 1 and channel 2 of NOAA-16's AVHRR instrument complicates *ex post facto* calibration. Thermal calibration coefficients after Weinreb *et al.* (1990) were used for the calibration of all thermal channels. (Weinreb et al. 1990)

### **9.2.3.2 Atmospheric Correction and Cloud Screening**

We choose to produce a maximum value NDVI composite data set, and associated layers, without any atmospheric correction, except during the El Chichon and Mt. Pinatubo volcanic stratospheric aerosol periods. A stratospheric aerosol correction was applied as proposed by Vermote *et al.* (1997) from April 1982 through December 1984 and from June 1991 through December 1994. We formed composite stratospheric aerosol optical depth fields by combining the work of Sato *et al.* (1993), and Vermote *et al.* (1997). Rosen *et al.* (1994), Russel et al. (1993) and Dutton (1994) were used to compare specific optical depth measurements to our blended global fields. We produced optical depth fields that varied by month and degree of latitude.

Cloud screening was provided by a channel 5 thermal mask of 0° C for all continents except Africa, where a cloud mask of 10° C was used. In addition, the bimonthly composites significantly reduced cloud contamination and the channel 4 and channel 5 thermal values are available for *ex post facto* cloud screening if desired.

### **9.2.3.3 Satellite drift correction using Pinzon et al (2002) method**

The GIMMS group uses Empirical Mode Decomposition (EMD) to identify and remove parts of the NDVI signal that are most related to the satellite drift (Pinzon 2002; Pinzon et al. 2004) The EMD technique was introduced by Nordon Huang in 1998 as an alternative to standard decomposition techniques for representation of nonlinear and nonstationary data that show clear physical scales or frequency content. Unlike Fourier decomposition (Wilks 1995; Trefethen and Bau 1997), the EMD a basis for the signal from the data itself. The EMD is empirical, intuitive, direct, *a posteriori*, and adaptive, with the decomposition functions based on and derived from the data (Huang et al. 1998; Huang et al. 1999). Pinzon et al. (2001) showed that EMD was applicable to NDVI time series from the AVHRR sensor to isolate orbital drift effects from the NDVI signal.(Pinzon et al. 2001)

Orbital drift results in later equatorial crossing times for the NOAA satellites and results in changes of illumination that affect the NDVI. In this dataset, we identify the trends in the NDVI that associated with changes in sun-target-sensor geometry due to satellite drift. Figure 3 shows the

*Global Inventory Modeling and Mapping Studies (GIMMS) AVHRR 8km Normalized Difference Vegetation Index (NDVI), Bimonthly 1981-2006.*

effects of satellite drift on the Solar Zenith Angle (SZA) at three latitude bands, 75-35N, 35N-35S and 35S-55S. An increasing trend is observed in each satellite due to its delay in the equatorial crossing time. This trend, superimposed on each plot, is more pronounced at lower latitude, whereas seasonal variations dominate at higher latitudes. Note that equatorial latitudes have an extra oscillation due to solar nadir moving past the target latitude, causing an increase in SZA at six month intervals rather than at yearly intervals (Privette et al. 1995).

The EMD is used to extract NDVI trends that may be caused by the satellite orbital drift, reducing the interference of other components in the NDVI signal. The EMD is used to isolate the components of the NDVI signal that are related to SZA trends and remove them from the corrected NDVI (see Figures 2 and 3). The technique removes NDVI trends that are more than 80% correlated to the SZA trends shown in Figure 2. Areas with trends that have a lower correlation are not corrected. Figure 3 shows both cases: trend removal from NDVI signal due to high correlation with the satellite drift, and trends that have not been altered because of low correlation to satellite drift.

Figure 4 shows areas where the correction is the strongest, notably 1) the tropics are most affected by satellite drift due to the SZA trend magnitudes, and 2) the high northern latitude and regions with low vegetation biomes are less contaminated since the SZA component represents a small part of the NDVI signal (see Figure 2). The correction is performed by-pixel. After the satellite drift correction, a kriging interpolation removes noise and attenuates the effect of cloudy and missing pixels.

#### **9.2.3.4 Intercalibration of NDVI from all instruments using narrow-band instruments such as MODIS and SPOT-Vegetation**

In order to include the data from NOAA-16, an intercalibration of the single-gain satellites NOAA-7-14 (historical data) and the dual-gain NOAA-16 with data from SPOT-Vegetation global data at 1 km (AcharDET al. 1992). SPOT data was averaged from 1 km to 8 km globally and then decomposed using the EMD method. The interannual trend from three years of data, 20 months overlapping with NOAA-14 and the rest with NOAA-16, was extracted. This trend was determined to be invariant through time over the period examined. A similar trend was extracted from the same period of NOAA-14. A non-linear regression was performed to establish coefficients that transform the historical data into the same range as that of the current and upcoming suite of visible and NIR sensors, such as MODIS, SPOT-Vegetation and others (Morissette et al., 2004). A similar regression was performed for the NOAA-16 data. Once the trends from the historical and NOAA-16 data were transformed into the common range, the data was reconstructed and a consistent time series was established.

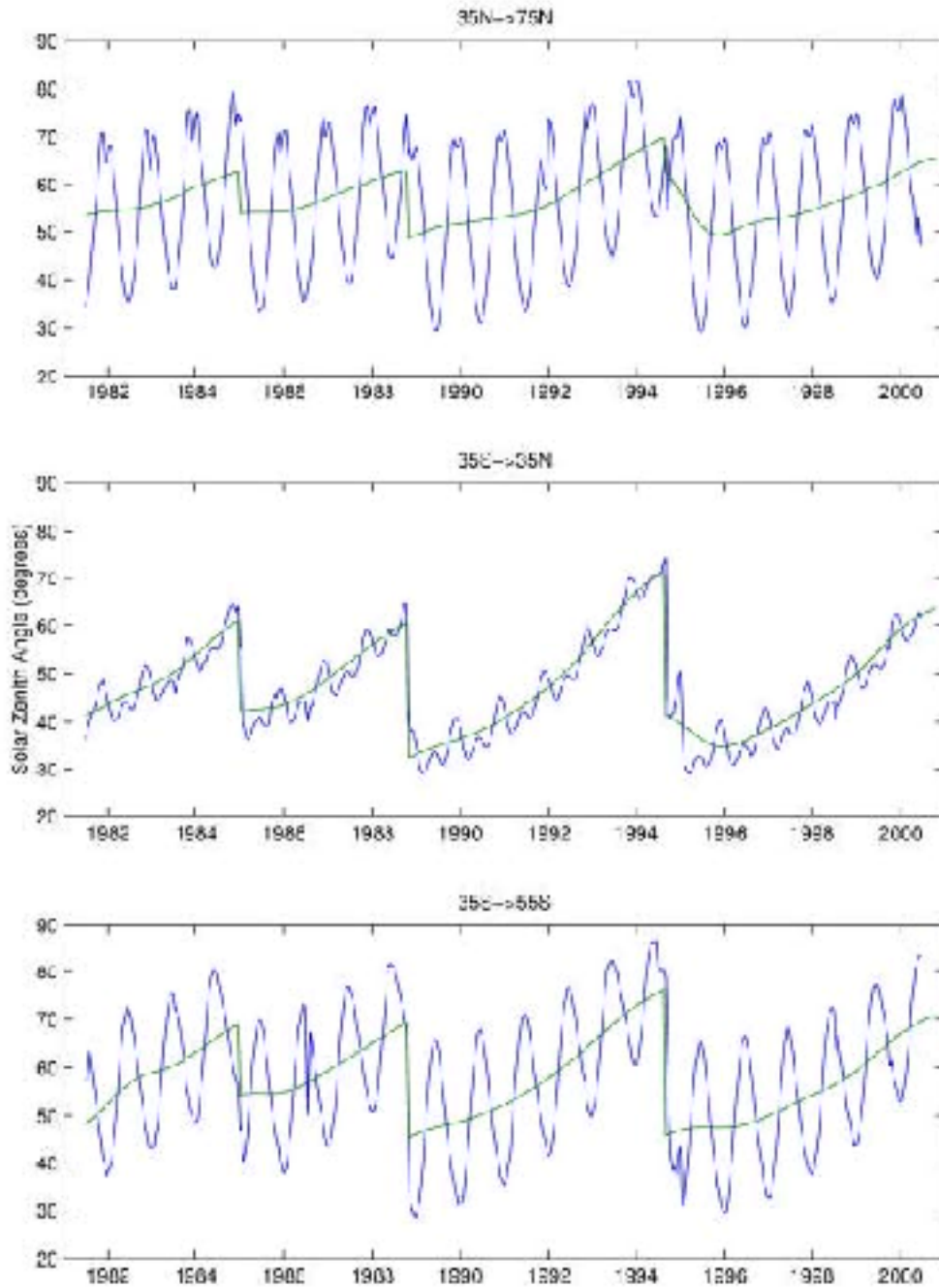


**Figure 2.** Solar Zenith Angles and trends derived from the NOAA-AVHRR sensor, averaged by latitude bands 75N-35N, 35N-5S, 35S-55S

A. B.

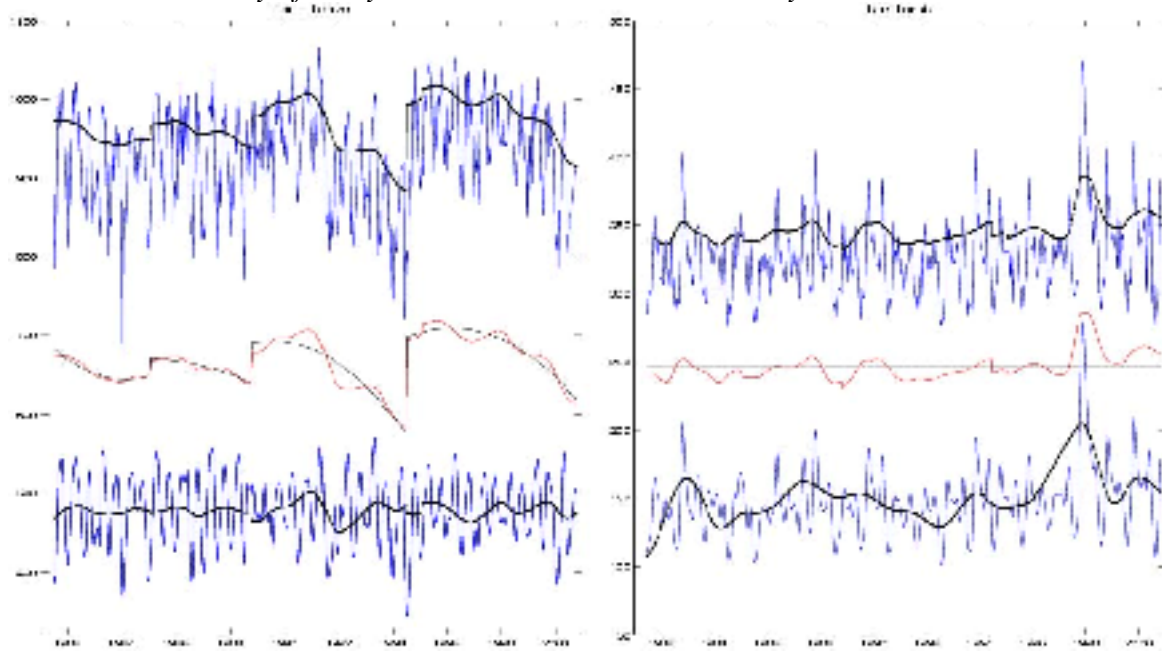


**Figure 3.** EMD decomposition and removal of SZA-correlated trends. A. Before satellite drift correction (series at top), trend removed (middle) and resulting series (bottom). B. Example of a pixel that is not corrected due to lack of correlation with the SZA trends.

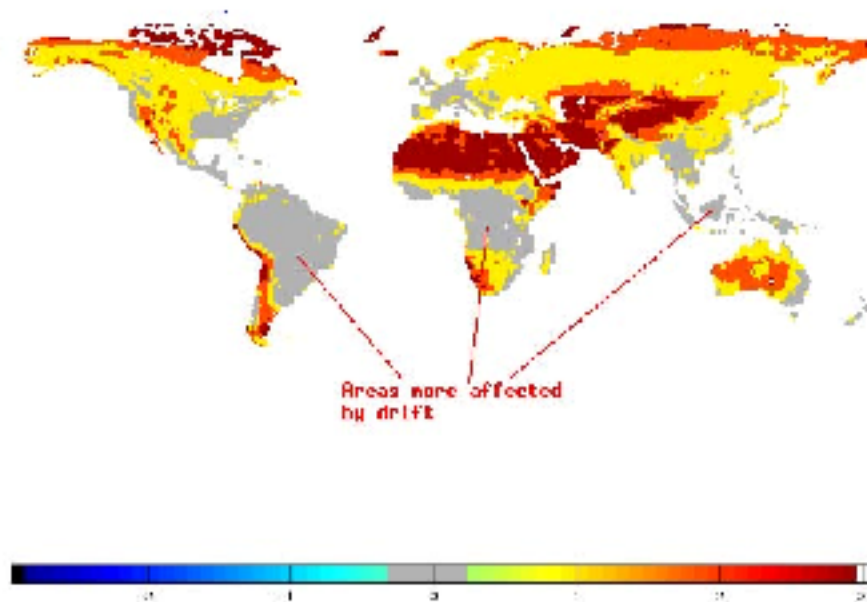


**Figure 4.** Regions where satellite drift has an important contribution to the signal.

### 9.3 Calculations

#### 9.3.1 Special Corrections/Adjustments

None other than those described in 9.1 and 9.2 above.

*Global Inventory Modeling and Mapping Studies (GIMMS) AVHRR 8km Normalized Difference Vegetation Index (NDVI), Bimonthly 1981-2006.*

## **9.4 Graphs and Plots**

See text above, Tucker et al. (2003), Pinzon et al. (2003) for some graphs and plots of the data.

## **10. ERRORS**

### **10.1 Sources of Error**

Some sources of error in the NDVI data set are not accounted for with the GIMMS corrections. These errors are caused by:

- soil background reflectance; this affects low NDVI values, but does not affect high NDVI values. Thus similar low NDVI values may indicate different amounts of vegetation. However, the EMD noise removal diminishes it.

### **10.2 Quality Assessment**

#### **10.2.1 Data Validation by Source**

Earlier versions of the GIMMS-NDVI data have been used in various models and seem to capture general patterns of vegetation well. Tests on sites showed reasonable agreement of interannual variation in GIMMS NDVI and other measures of vegetation (Davenport and Nicholson 1993; Malmstrom et al. 1997; D'Arrigo et al. 2000). These tests show that the variation in GIMMS NDVI is realistic on specific sites. Comparison between climate signals and GIMMS NDVI show realistic patterns in many semi-arid regions and temperate regions.

Recent independent research has verified the quality of the NDVI data:

- Lotsch et al (2003a) using the new GIMMS NDVI presented here and global standardized precipitation index (SPI) data revealed geographically extensive patterns of joint NDVI-SPI variability (Lotsch et al. 2003).
- Jia et al (2003) analyzed the GIMMS NDVI data for three bioclimate subzones in northern Alaska and confirmed a long-term trend of increase in vegetation greenness for the Alaskan tundra that has been detected globally for the northern latitudes. There was a 16.9% ( $\pm 5.6\%$ ) increase in peak vegetation greenness across the region that corresponded to simultaneous increases in temperatures (Jia et al. 2003).
- In the Amazon basin, a recent publication by Poveda and Salazar (2004) showed that at interannual timescales, the NDVI shows a reaction to both phases of ENSO. Dryness was seen due to El Niño, whereas NDVI spatial variability is enhanced during La Niña (Poveda and Salazar 2004).
- Lotsch et al (2003b) demonstrated that seasonal GIMMS-NDVI anomalies for Africa, spatial independent component analysis (ICA) reveals coherent regions that capture high interannual variability in arid and semiarid areas of eastern and southern Africa that were associated with fluctuations in sea surface temperature anomalies (SSTA). When using other AVHRR datasets (here, PAL) known to be contaminated with volcanic aerosols and sensor transition discontinuities, Lotsch et al (2003b) needed to apply ICA correction to account for these artifacts. When using these other datasets, results must be treated with caution (Lotsch et al. 2003).
- Nemani et al (2002) found a 6% increase in NPP using the GIMMS NDVI in their primary production model corresponding with known corresponding with changes in CO<sub>2</sub> concentrations 42% of the increase was from tropical forests due to decreases in cloud cover. Their satellite-based estimates of NPP show significant growth stimulation in both the tropics and the northern high-latitude ecosystems. Assuming that carbon emissions, including those from biomass

burning and land-use changes, are properly accounted for in the atmospheric inversions, this spatial discrepancy means that respiration as well as NPP is a major driver of terrestrial carbon-sink dynamics (Nemani et al. 2002).

### **10.2.2 Confidence Level/Accuracy Judgment**

The GIMMS-NDVI data set is believed to give large improvements over the Pathfinder NDVI data set, especially for areas with persistent cloud cover and for needle bearing evergreen vegetation during winter. GIMMS-NDVI has reduced the effects of orbital drift, which are especially large near the end of the time of operation a satellite. Corrections for atmospheric aerosols are likely to be too small from about one to three months after an eruption (May-Jul 1982 for El Chichon and Jul-Sep 1991 for Mt Pinatubo), where the aerosols have not mixed evenly into the atmosphere (Brown et al. 2003).

### **10.2.3 Measurement Error for Parameters and Variables**

None given.

### **10.2.4 Additional Quality Assessment Applied**

NDVI data are increasingly being used to assess interannual variations in the biosphere; we would like to distinguish between the following types of temporal analysis (see also Gutman 1995) (Gutman et al. 1995):

- seasonal analysis: NDVI data should have more than sufficient accuracy to assess seasonality of vegetation with great confidence. The one exception may be the small seasonal cycles observed in the Sahara, this seasonality is most likely caused by variations in atmospheric water vapor, not by variations in vegetation.
- interannual analysis: NDVI data have been used to look at year-to-year variations in desert margins (Tucker et al. 1991) and to variations associated with climate oscillations (Myneni et al. 1995). The interannual signal in semi-arid regions and temperate regions is in general larger than the residual errors in the data.
- trend analysis: This is in general the smallest interannual signal in the data; errors in the NDVI data are often as large or larger than the magnitude of trends, at this stage the magnitude of trends in NDVI data is uncertain within an order of magnitude.

## **11. NOTES**

### **11.1 Known Problems with the Data**

The decline in NDVI in mid-1991 was due to the Pinatubo eruption and subsequent cooling and may not be related to actual declines in vegetation. Trends in tropical regions are affected by this decline and should therefore be treated with caution. In the high northern latitude (north of 65 degrees N) have been corrected for extremely high solar zenith angles during the winter months, and thus these values should be treated with caution. Data during the second half of 1994 and during most of 2000 had either unusually early or late overpass times and thus data from these periods should be used with caution.

### **11.2 Usage Guidance**

GIMMS NDVI presents generalized patterns that may result in poor representations of a specific locale, quantitative conclusions should be drawn with caution. Nevertheless, this NDVI dataset should provide a large improvement over previously used NDVI data sets, because the data are collected by one series of instruments, and they give a more realistic representation of the

*Global Inventory Modeling and Mapping Studies (GIMMS) AVHRR 8km  
Normalized Difference Vegetation Index (NDVI), Bimonthly 1981-2006.*

*University of Maryland Global Land Cover Facility Data Distribution*  
spatial and temporal variability of vegetation patterns over the globe. Users of the data are strongly encouraged to validate their results on independent data.

### **11.3 Other Relevant Information**

Not available at this revision.

## **12. REFERENCES**

### **12.1 Satellite/Instrument/Data Processing Documentation**

Kidwell, K. B. (1998). Polar Orbiter Data Users' Guide (TIROS-N, NOAA-6, NOAA-7, NOAA8, NOAA-9, NOAA-10, NOAA-11, NOAA-12, NOAA-14), National Oceanic and Atmospheric Administration. <http://www2.ncdc.noaa.gov/docs/podug/>.

Kidwell, K. B. (2000). NOAA KLM User's Guide, National Oceanic and Atmospheric Administration. <http://www2.ncdc.noaa.gov/docs/klm/>.

Pinzon, J., Brown, M.E. and Tucker, C.J., 2005. Satellite time series correction of orbital drift artifacts using empirical mode decomposition. In: N. Huang (Editor), Hilbert-Huang Transform: Introduction and Applications, pp. 167-186.

Tucker, C.J., Pinzon, J.E., Brown, M.E., Slayback, D., Pak, E.W., Mahoney, R., Vermote, E. and Saleous, N., 2005. An Extended AVHRR 8-km NDVI Data Set Compatible with MODIS and SPOT Vegetation NDVI Data. *International Journal of Remote Sensing*, 26(20): 4485-4498.

### **12.2 Journal Articles and Study Reports.**

Achard, F., J.-P. Malingreau, et al. (1992). A mission for global monitoring of the continental biosphere: the "Vegetation" Instrument on board "SPOT 4". Toulouse, France, LERTS.

Baldwin, D. and W. J. Emory (1995). "Spacecraft altitude variations in NOAA-11 infrared from AVHRR imagery." *International Journal of Remote Sensing* **16**: 531-548.

Brown, M.E., Pinzon, J.E., Didan, K., Morisette, J.T. and Tucker, C.J., 2006. Evaluation of the consistency of long-term NDVI time series derived from AVHRR, SPOT-Vegetation, SeaWiFS, MODIS and LandSAT ETM+. *IEEE Transactions Geoscience and Remote Sensing*, **44**(1): 1787-1793..

D'Arrigo, R. D., C. M. Malmstrom, et al. (2000). "Correlation between maximum latewood density of annual tree rings and NDVI based estimates of forest productivity." *International Journal of Remote Sensing* **21**(11): 2329-2336.

Davenport, M. L. and S. E. Nicholson (1993). "On the Relation between Rainfall and the Normalized Difference Vegetation Index for Diverse Vegetation Types in East Africa." *International Journal of Remote Sensing* **14**(12): 2369-2389.

Dutton, E. (1994). Aerosol optical depth measurements from four NOAA/CMDL monitoring sites. *Global Inventory Modeling and Mapping Studies (GIMMS) AVHRR 8km Normalized Difference Vegetation Index (NDVI), Bimonthly 1981-2006*.

*University of Maryland Global Land Cover Facility Data Distribution*  
Oak Ridge, Tennessee, Carbon Dioxide Information Analysis Center, Oak Ridge National  
Laboratory: 484-494.

El Saleous, N. Z., E. F. Vermote, et al. (2000). "Improvements in the global biospheric record from the Advanced Very High Resolution Radiometer (AVHRR)." International Journal of Remote Sensing **21**(6-7): 1251-1277.

Emery, W. J., J. Brown, et al. (1989). "AVHRR Image Navigation: Summary and Review." Photogrammetric Engineering and Remote Sensing **55**: 1175-1183.

Gutman, G., D. Tarpley, et al. (1995). "The enhanced NOAA Global land dataset from the Advanced Very High Resolution Radiometer." Bulletin American Meteorological Society **76**(7): 1141-1156.

Huang, N. E., Z. Shen, et al. (1999). "A new view of nonlinear water waves: the Hilbert spectrum." Annual Review of Fluid Mechanics **31**: 417-457.

Huang, N. E., Z. Shen, et al. (1998). "The empirical mode decomposition and the Hilbert spectrum for nonlinear and non-stationary time series analysis." Proceedings of the Royal Society of London **545**: 903-995.

Jia, G. S. J., H. E. Epstein, et al. (2003). "Greening of arctic Alaska, 1981-2001." Geophysical Research Letters **30**(20).

Kidwell, K. B. (1998). Polar Orbiter Data Users' Guide (TIROS-N, NOAA-6, NOAA-7, NOAA8, NOAA-9, NOAA-10, NOAA-11, NOAA-12, NOAA-14). Washington D.C., National Oceanic and Atmospheric Administration.

Los, S. O. (1998). "Estimation of the Ratio of Sensor Degradation Between NOAA AVHRR Channels 1 and 2 from Monthly NDVI Composites." IEEE Transactions on Geoscience and Remote Sensing **36**(1): 206-213.

Lotsch, A., M. A. Friedl, et al. (2003). "Coupled vegetation-precipitation variability observed from satellite and climate records." Geophysical Research Letters **30**(14).

Lotsch, A., M. A. Friedl, et al. (2003). "Spatio-Temporal Deconvolution of NDVI Image Sequences Using Independent Component Analysis." IEEE Transactions Geoscience and Remote Sensing **41**(12): 2938-2942.

Malmstrom, C. M., M. V. Thompson, et al. (1997). "Interannual variation in global-scale net primary production: Testing model estimates." Global Biogeochemical Cycles **11**(3): 367-392.

Myneni, R. B., F. G. Hall, et al. (1995). "The Interpretation of Spectral Vegetation Indexes." Ieee Transactions on Geoscience and Remote Sensing **33**(2): 481-486.

Morisette, J.T., Pinzon, J.E., Brown, M.E., Tucker, C.J. and Justice, C.O., 2004. Initial validation of NDVI time series from AVHRR, Vegetation and MODIS, Proceeding of the 2nd SPOT

*Global Inventory Modeling and Mapping Studies (GIMMS) AVHRR 8km  
Normalized Difference Vegetation Index (NDVI), Bimonthly 1981-2006.*

*University of Maryland Global Land Cover Facility Data Distribution*  
VEGETATION Users conference, Antwerp, Belgium, pp. 149-154.

Nemani, R., M. White, et al. (2002). "Recent trends in hydrologic balance have enhanced the terrestrial carbon sink in the United States." Geophysical Research Letters **29**(10).

Pinzon, J. (2002). Using HHT to successfully uncouple seasonal and interannual components in remotely sensed data. SCI 2002 Conference Proceedings Jul 14-18, Orlando, Florida, SCI International.

Pinzon, J., M. E. Brown, et al. (2004). Satellite time series correction of orbital drift artifacts using empirical mode decomposition. Hilbert-Huang Transform: Introduction and Applications. N. Huang: Chapter 10, Part II. Applications.

Pinzon, J., J. F. Pierce, et al. (2001). Analysis of Remote Sensing Data Using Hilbert-Huang Transform. SCI 2001 Conference Proceedings.

Poveda, G. and L. F. Salazar (2004). "Annual and Interannual (ENSO) Variability of Spatial Scaling Properties of a Vegetation Index (NDVI) in Amazonia." Remote Sensing of Environment **in press**.  
Privette, J. L., C. Fowler, et al. (1995). "Effects of Orbital Drift on Advanced Very High Resolution Radiometer Products: Normalized Difference Vegetation Index and Sea Surface Temperature." Remote Sensing of Environment **53**: 164-171.

Rao, C. R. N. and J. Chen (1995). "Inter-satellite calibration linkages for the visible and near-infrared channels of the Advanced Very High Resolution Radiometer on the NOAA-7, -9, and 11 spacecraft." International Journal of Remote Sensing **16**: 1931-1942.

Rosen, J. M., N. T. Kjome, et al. (1994). "Decay of Mount Pinatubo aerosol at midlatitudes in the northern and southern hemispheres." Journal of Geophysical Research **99**(D12): 25733-25739.

Russel, P. B., J. M. Livingston, et al. (1993). "Pinatubo and pre-Pinatubo optical-depth spectra: Mauna Loa measurements, comparisons, inferred particle size distributions, radiative effects, and relationships to lidar data." Journal of Geophysical Research **98**: 22969-22985.

Sato, M., M. Hansen, et al. (1993). "Stratospheric Aerosol Optical Depths, 1850-1990." Journal of Geophysical Research **98**(D12): 22987-22994.

Sellers, P., C. J. Tucker, et al. (1994). "A global 1 degree x 1 degree NDVI data set for climate studies. Part 2." International Journal of Remote Sensing **15**(17): 3519-3545.

Sellers, P. J. (1985). "Canopy Reflectance, Photosynthesis, and Transpiration." International Journal of Remote Sensing **6**(8): 1335-1372.

Trefethen, L. N. and D. Bau (1997). Numerical Linear Algebra. Philadelphia, Society for Industrial and Applied Mathematics.

Tucker, C. J. (1980). "Remote Sensing of Leaf Water Content in the Near Infrared." Remote Sensing of Environment **10**: 23-32.

*Global Inventory Modeling and Mapping Studies (GIMMS) AVHRR 8km  
Normalized Difference Vegetation Index (NDVI), Bimonthly 1981-2006.*

*University of Maryland Global Land Cover Facility Data Distribution*

Tucker, C. J., H. E. Dregne, et al. (1991). "Expansion and Contraction of the Sahara Desert from 1980 to 1990." Science **253**: 299-301.

Tucker, C.J., Pinzon, J.E., Brown, M.E., Slayback, D., Pak, E.W., Mahoney, R., Vermote, E. and Saleous, N., 2005. An Extended AVHRR 8-km NDVI Data Set Compatible with MODIS and SPOT Vegetation NDVI Data. International Journal of Remote Sensing, 26(20): 4485-4498.

Vermote, E., N. El Saleous, et al. (1997). "Data Pre-Processing: Stratospheric Aerosol Perturbing Effect on the Remote Sensing of Vegetation: Correction Method for the Composite NDVI after the Pinatubo Eruption." Remote Sensing Reviews **15**: 7-21.

Vermote, E. and Y. J. Kaufman (1995). "Absolute calibration of AVHRR visible and near-infrared channels using ocean and cloud views." International Journal of Remote Sensing **16**(13): 2317-2340.

Weinreb, M. P., G. Hamilton, et al. (1990). "Nonlinearity corrections in calibration of Advanced Very High Resolution Radiometer infrared channels." Journal of Geophysical Research **95**: 7381-7388.

Wilks, D. S. (1995). Statistical Methods in the Atmospheric Sciences, an Introduction. San Diego, Academic Press.